ChemComm

Cite this: *Chem. Commun.*, 2011, **47**, 5512–5514

www.rsc.org/chemcomm

COMMUNICATION

Exceptional visible-light-driven photocatalytic activity over BiOBr–$ZnFe_2O_4$ heterojunctions†

Liang Kong,[a] Zheng Jiang,*[ab] Tiancun Xiao,[a] Lufeng Lu,[a] Martin O. Jones[ac] and Peter P. Edwards*[a]

Received 23rd January 2011, Accepted 16th March 2011
DOI: 10.1039/c1cc10446b

An ultrasound-assisted, precipitation–deposition method has been developed to synthesise visible-light-responsive BiOBr–$ZnFe_2O_4$ heterojunction photocatalysts. The heterojunctions with suitable BiOBr/$ZnFe_2O_4$ ratios have a fascinating micro-spherical morphology and exhibit exceptional photocatalytic activity in visible-light degradation of Rhodamine B.

The semiconductor BiOBr has recently stimulated intensive interest in solar energy conversion due to its high photocatalytic activity and stability under UV and visible light irradiation.[1–6] BiOBr is a lamellar-structured p-type semiconductor with intrinsic indirect band gap which endows it with excellent mobility and a prolonged transfer path for photogenerated electrons.[7] However, the band gap energy (E_g) of BiOBr is around 2.9 eV, indicating that it cannot absorb a significant part of visible-light above 430 nm.[8]

Impurity doping is an effective and the most frequently used method to extend the optical absorption edge of wide band gap semiconductors.[1,9–11] Indeed, the doping of BiOBr with I or Pb may narrow the band gap of BiOBr significantly.[6,12] However, the activity of doped photocatalysts is usually sensitive to both the doping level and homogeneity.[5] In contrast, combining two semiconductors with different band gaps to form heterojunctions, such as BiOCl/Bi_2O_3 and AgI/BiOI,[8,13] is more flexible than doping for broadening the visible-light absorption and less sensitive to the component homogeneity (*i.e.* better tolerance to component heterogeneity). This is because the heterojunction has great potential in tuning the desired electronic properties of the composite photocatalysts.[8] Though AgX (X = Cl, Br, I) are frequently used in building heterojunctions with suitable semiconductors, they usually suffer from significant deactivation.[8,13,14]

Zinc ferrite ($ZnFe_2O_4$) is a spinel-type (AB_2O_4) semiconductor with a typical E_g of about 1.9 eV, which enables it to absorb sunlight up to 653 nm or even larger.[15] Despite the fact that $ZnFe_2O_4$ itself has very little activity due to the rapid recombination of light-excited charges, it shows good stability in photodegradation of organics.[16] Enhanced visible-light-driven photoactivity has been observed over some composite semiconductors which combine $ZnFe_2O_4$ with secondary semiconductor, such as TiO_2 or ZnO, of large E_g.[5] These results motivated us to fabricate BiOBr–$ZnFe_2O_4$ heterojunctions with the hope of enhanced catalytic performance.

Here we report a class of novel p–n heterostructures comprising of n-type $ZnFe_2O_4$ and p-type BiOBr. The BiOBr–$ZnFe_2O_4$ heterojunctions were prepared *via* a simple ultrasound deposition method. Briefly, the $ZnFe_2O_4$ was dispersed into the $Bi(NO_3)_3$ solution prior to adding the mixture into a solution containing stoichiometric KBr under ultrasonication. The obtained catalysts were characterised using X-Ray Diffraction (XRD), Scanning Electron Microscopy (SEM), Transmission Electron Microscopy (TEM), Energy-Dispersive X-ray Spectroscopy (EDS) and UV-Visible spectroscopy techniques. The catalysts showed preeminent activity in the visible-light-driven photodegradation of Rhodamine B (RhB). The experimental details are included in the ESI.†

The XRD patterns (Fig. 1) of the as-synthesised samples can be indexed to $Fd\bar{3}m$ cubic $ZnFe_2O_4$ (JCPDS 21-874)[17] and $P4/nmm$ tetragonal BiOBr (JCPDS 73-2061)[18] crystal phases, respectively. The narrow and sharp Bragg diffractions of each component reveal that BiOBr and $ZnFe_2O_4$ in the samples are highly crystalline.[17] No other phases can be found in the BiOBr–$ZnFe_2O_4$ heterojunctions, suggesting that no impurity species were formed between BiOBr and $ZnFe_2O_4$.[8] However, the average crystallite sizes of BiOBr in the heterojunctions are much smaller than that of pure BiOBr as shown in Table 1,

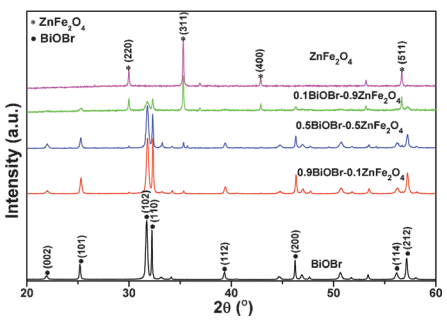

Fig. 1 XRD patterns of as-synthesised BiOBr–$ZnFe_2O_4$ samples.

[a] *Department of Chemistry, Inorganic Chemistry Laboratory, University of Oxford, Oxford, UK OX1 3QR. E-mail: peter.edwards@chem.ox.ac.uk; Tel: +44 (0)1865 272646*
[b] *Jesus College, University of Oxford, Oxford, UK OX1 3DW. E-mail: zhjiang76@hotmail.com; Tel: +44 (0)1865 272660*
[c] *Rutherford Appleton Laboratory, Harwell Science and Innovation Campus, Didcot, UK*

† Electronic supplementary information (ESI) available: Experimental protocols and product characterization. See DOI: 10.1039/c1cc10446b

Table 1 The average crystallite sizes, E_g and photodegradation rate constants (k_{RhB}) of BiOBr–$ZnFe_2O_4$ composite photocatalysts

Photocatalyst	Crystallite size[a]/nm	E_g[b]/eV	k_{RhB}/min^{-1}
BiOBr	107.3	2.88	0.070
0.9BiOBr–0.1$ZnFe_2O_4$	75.1	2.13	0.201
0.7BiOBr–0.3$ZnFe_2O_4$	34.6	2.01	0.083
0.5BiOBr–0.5$ZnFe_2O_4$	27.9	2.25	0.148
0.1BiOBr–0.9$ZnFe_2O_4$	37.6	1.71	0.019
$ZnFe_2O_4$	83.4	1.67	0.001
TiO_2	—	3.20[3]	0.012
Mechanically mixed 0.9BiOBr–0.1$ZnFe_2O_4$	—	—	0.095

[a] Calculated from the Scherrer equation. [b] E_g was derived from $E_g = 1239.8/\lambda_g$, where λ_g is the absorption edge in the UV-Vis spectra.[4]

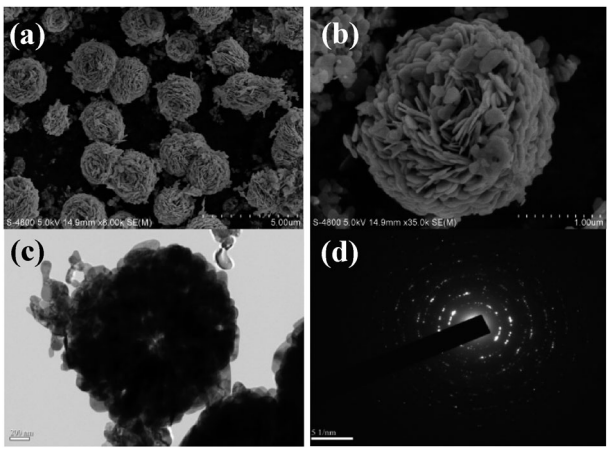

Fig. 2 (a, b) FESEM images of the 0.9BiOBr–0.1$ZnFe_2O_4$ sample at low and high magnification; (c, d) TEM and SAED images of 0.9BiOBr–0.1$ZnFe_2O_4$.

revealing the crystallite size of BiOBr may be attenuated by the surface deposition onto $ZnFe_2O_4$. The preferential crystal plane of the ultrasonication-deposited BiOBr is (110) rather than (102) crystal plane for BiOBr synthesized by co-precipitation.[4]

The morphology and composition of the BiOBr–$ZnFe_2O_4$ were analysed by SEM, TEM, and EDS. The low-magnification SEM image reveals that a typical 0.9BiOBr–0.1$ZnFe_2O_4$ sample consists of a large number of particles with micro-spherical structure (Fig. 2a). The high-resolution SEM image of an individual particle (0.9BiOBr–0.1$ZnFe_2O_4$, Fig. 2b) shows that the outer part of the microsphere is constructed by numerous thin flakes with a thickness of about 20 nm, which aggregated together to form the hierarchical assembly.[3] EDS analysis of the microsphere reveals that Bi, O, Br, Zn and Fe elements coexist in the BiOBr–$ZnFe_2O_4$ composite materials (ESI†). The TEM image of the 0.9BiOBr–0.1$ZnFe_2O_4$ composite sample further verifies that the microspheres are built with many nanoflakes (Fig. 2c). It can be inferred that the individual nanoflakes were formed and aggregated on the surface of $ZnFe_2O_4$ under the ultrasound deposition process to form the hierarchical spheres. The TEM image of single microsphere illustrates that it has a hollow centre. The selected area electron diffraction (Fig. 2d) of the assembly suggests that the BiOBr–$ZnFe_2O_4$ composites are polycrystalline including both BiOBr and $ZnFe_2O_4$.[3]

In order to understand the formation conditions of the micro-spherical morphology of BiOBr–$ZnFe_2O_4$, SEM images of the sample with different BiOBr/$ZnFe_2O_4$ ratios were conducted. The spherical morphology disappeared once the BiOBr/$ZnFe_2O_4$ ratio is less than one, because BiOBr cannot fully cover the surface of $ZnFe_2O_4$ particles. For example, numerous irregularly arranged nano-plates are observed in the SEM image of 0.5BiOBr–0.5$ZnFe_2O_4$ (Fig. S1a, ESI†). On the basis of the SEM observation, we proposed the growth and assembly process of the heterojunctions along with the component molar ratio. BiOBr is prone to aggregating into stacked plates without secondary particles existing in the synthetic solution (Fig. S6, ESI†). Given that a suitable amount of $ZnFe_2O_4$ added into the solution, BiOBr flakes will deposit uniformly on the surface of $ZnFe_2O_4$, which serves as 'seeds' in the ultrasound-assisted deposition process, and grows to form a spherical assembly of the BiOBr flaked blocks around the seed. Once the added seeds exceed the desired amount for spherical assembly, the BiOBr flakes cannot fully cover the seeds, leading to irregular morphologies. The gradual change of the colour in the synthetic solutions and UV-Vis spectra also provides some evidence to support this assumption.

Fig. 3a shows the activity of RhB photodegradation on as-synthesised BiOBr–$ZnFe_2O_4$ composites under visible-light irradiation and Fig. 3b shows the absorption spectra variation of RhB *versus* irradiation time on the 0.9BiOBr–0.1$ZnFe_2O_4$ sample. The characteristic absorption band of RhB at 554 nm diminished quickly, accompanied by slight concomitant blue-shift from 554 to 494 nm of the maximum absorption. The rate constant per unit mass, k, of each photocatalyst is also listed in Table 1. All the photocatalysts showed some photocatalytic activity under visible-light irradiation but importantly RhB itself was not decomposed in the absence of the catalyst. Pure $ZnFe_2O_4$ showed weak reactivity, on which less than 10% RhB was decomposed in 90 min irradiation, which was even worse

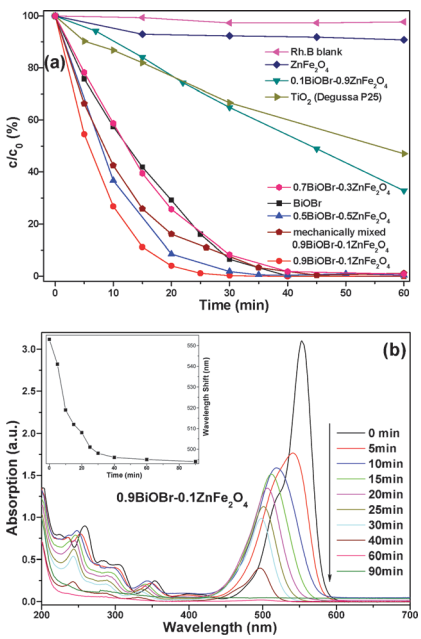

Fig. 3 (a) Photodegradation of RhB over BiOBr–$ZnFe_2O_4$ composites; (b) UV-Visible spectra of RhB *vs.* photoreaction time; wavelength shifts as a function of the decrease in absorption maximum (inset).

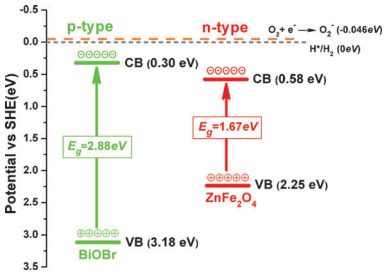

Fig. 4 A simplified band structure diagram for BiOBr and $ZnFe_2O_4$.

than P25 (Degussa TiO_2 aerosol). The photodegradation of RhB on P25 can be attributed to dye-sensitised photocatalysis since P25 cannot be activated by visible light.[4] The highest activity was observed over the 0.9BiOBr–0.1$ZnFe_2O_4$ sample, on which about 73% RhB was degraded in the first 10 minutes of visible-light irradiation. The photoreaction kinetics constant on the best catalyst is around 3 times and 200 times of those of pure BiOBr and $ZnFe_2O_4$ samples, respectively. Although the activity of the composite catalysts decreases as the amount of $ZnFe_2O_4$ increases, 0.1BiOBr–0.9$ZnFe_2O_4$ is still much better than $ZnFe_2O_4$ and is comparable to P25.

The k_{RhB} values are not proportional to the molar ratio of BiOBr/$ZnFe_2O_4$, suggesting that the coexistence of $ZnFe_2O_4$ and BiOBr gives rise to some positive synergy for the BiOBr–$ZnFe_2O_4$ heterostructures. From the electronic structure point of view, as depicted in Fig. 4, the band potentials of BiOBr and $ZnFe_2O_4$ in the heterostructures fit the requirements to form a heterojunction with a straddling gap, which may facilitate the transfer of charge carriers and retard the e^-–h^+ recombination, resulting in improved photocatalytic performance. The potentials of conductance and valence band (CB and VB) edges of BiOBr and $ZnFe_2O_4$ were estimated *via* Mulliken electronegativity theory:[19] $E_{VB} = X_{semiconductor} - E^0 + 0.5E_g$, where E_{VB} is the VB edge potential, $X_{semiconductor}$ is the electronegativity of the semiconductor, which is the geometric mean of the electronegativity of the constituent atoms, E^0 is the standard electrode potential on the hydrogen scale (*ca.* 4.5 eV). The VB of $ZnFe_2O_4$ may partially accept the excited electrons from VB of BiOBr and thereby stabilise its photogenerated holes. The photogenerated holes have a strong oxidation potential and serve as active sites responsible for RhB photodegradation.[4] Furthermore, $ZnFe_2O_4$ is also a sensitiser which considerably broadens the light absorption edges of the heterojunctions in visible-light regions, and may provide photogenerated electrons to sensitise BiOBr.[20] However, $ZnFe_2O_4$ is significantly less active since its photogenerated charges are prone to recombination.[8] On the other hand, the superior reactivity of the BiOBr–$ZnFe_2O_4$ heterojunctions as compared to BiOBr were observed on samples with appropriate molar ratios of $ZnFe_2O_4$ to BiOBr, suggesting that there is a critical ratio for such a positive synergistic effect. Above this critical ratio, excessive $ZnFe_2O_4$ covers the active sites of BiOBr and hinders the visible-light penetration in the sample to excite BiOBr. This correspondingly deteriorates the photocatalytic activity, as a consequence of less available BiOBr and increased recombination of the photogenerated charges on $ZnFe_2O_4$.

The heterojunction effect can only occur on closely contacted interfaces within the samples.[21] Indeed, enhanced reactivity was observed for the synthesised 0.9BiOBr–0.1$ZnFe_2O_4$ heterojunction than for the mechanically mixed 0.9BiOBr–0.1$ZnFe_2O_4$ sample (Fig. 3a) because the latter has more loosely contacted interfaces. The activity of the mechanically mixed 0.9BiOBr–0.1$ZnFe_2O_4$ is higher than BiOBr, which can be depicted in terms of the Z-schemed photocatalysts in an aqueous solution,[22] where the photocharges may transfer between the two semiconductors with different band gaps. Here, the Z-scheme system can improve the electron separation *via* the aqueous medium but is less efficient than the corresponding heterojunctions due to the distance limit of the charge transfer.[11] Hence, the enhanced reactivity of the suitable BiOBr–$ZnFe_2O_4$ p–n junctions can be reasonably assigned to the well-aligned straddling band-structures of the BiOBr–$ZnFe_2O_4$ upon their intimately contacted interfaces.

We greatly acknowledge financial support from the John Houghton Research Fellowship and Principal's Major Research Fund at Jesus College, Oxford. Z. J. appreciates the international travelling and collaboration grants (TG092414 and TG101750) from the Royal Society, UK. We thank Nanjing University of Technology for the help with SEM and TEM. We also thank Prof. M. Croker and Ms. A. Harman at CAER, University of Kentucky, US, for their helpful discussions.

Notes and references

1 Z. Jiang, T. Xiao, V. L. Kuznetsov and P. P. Edwards, *Philos. Trans. R. Soc. London, Ser. A*, 2010, **368**, 3343–3364.
2 J. Zhang, F. Shi, J. Lin, D. Chen, J. Gao, Z. Huang, X. Ding and C. Tang, *Chem. Mater.*, 2008, **20**, 2937–2941.
3 Z. H. Ai, W. K. Ho, S. C. Lee and L. Zhang, *Environ. Sci. Technol.*, 2009, **43**, 4143–4150.
4 Z. Jiang, F. Yang, G. Yang, L. Kong, M. O. Jones, T. Xiao and P. P. Edwards, *J. Photochem. Photobiol., A*, 2010, **212**, 8–13.
5 Z. Shan, W. Wang, X. Lin, H. Ding and F. Huang, *J. Solid State Chem.*, 2008, **181**, 1361–1366.
6 W. Wang, F. Huang, X. Lin and J. Yang, *Catal. Commun.*, 2008, **9**, 8–12.
7 K. Zhu, N. R. Neale, A. Miedaner and A. J. Frank, *Nano Lett.*, 2007, **7**, 69–74.
8 S. Y. Chai, Y. J. Kim, M. H. Jung, A. K. Chakraborty, D. Jung and W. I. Lee, *J. Catal.*, 2009, **262**, 144–149.
9 R. Asahi, T. Morikawa, T. Ohwaki, K. Aoki and Y. Taga, *Science*, 2001, **293**, 269–271.
10 Z. Jiang, F. Yang, N. Luo, B. T. T. Chu, D. Sun, H. Shi, T. Xiao and P. P. Edwards, *Chem. Commun.*, 2008, 6372–6374.
11 J. H. Pan, H. Dou, Z. Xiong, C. Xu, J. Ma and X. S. Zhao, *J. Mater. Chem.*, 2010, **20**, 4512–4528.
12 C. Yu, J. C. Yu, C. Fan, H. Wen and S. Hu, *Mater. Sci. Eng., B*, 2010, **166**, 213–219.
13 H. Cheng, B. Huang, Y. Dai, X. Qin and X. Zhang, *Langmuir*, 2010, **26**, 6618–6624.
14 Y. Zang and R. Farnood, *Appl. Catal. B: Environ.*, 2010, **79**, 334–340.
15 Y. Hou, X.-Y. Li, Q.-D. Zhao, X. Quan and G.-H. Chen, *Adv. Funct. Mater.*, 2010, **20**, 2165–2174.
16 J. Qiu, C. Wang and M. Gu, *Mater. Sci. Eng., B*, 2004, **112**, 1–4.
17 S. Boumaza, A. Boudjemaa, A. Bouguelia, R. Bouarab and M. Trari, *Appl. Energy*, 2010, **87**, 2230–2236.
18 J. Ketterer and V. Kramer, *Acta Crystallogr., Sect. C: Cryst. Struct. Commun.*, 1986, **42**, 1098–1099.
19 A. H. Nethercot, *Phys. Rev. Lett.*, 1974, **33**, 1088.
20 Z.-h. Yuan and L.-d. Zhang, *J. Mater. Chem.*, 2001, **11**, 1265–1268.
21 O. Moutanabbir and U. Gosele, in *Annu. Rev. Mater. Res.*, Annual Reviews, Palo Alto, 2010, vol. 40, pp. 469–500.
22 H. Tada, T. Mitsui, T. Kiyonaga, T. Akita and K. Tanaka, *Nat. Mater.*, 2006, **5**, 782–786.